Materials Science Forum
ISSN: 0255-5476, Vol. 846, pp 614-619
doi:10.4028/www.scientific.net/MSF.846.614

Submitted: 2014-12-31
Revised: 2015-05-26
Accepted: 2015-10-08

Polarized Infrared Reststrahlen Features of Wurtzite InGaN Thin Film

Pauline Yew[1*], Lee Sai Cheong[1,2], Ng Sha Shiong[1], Yoon Tiem Leong[1], Haslan Abu Hassan[1], Wei-Li Chen[3]

[1]Institute of Nano-Optoelectronics Research and Technology (INOR), School of Physics, Universiti Sains Malaysia, 11800 Minden, Penang, Malaysia.

[2]Department of Physics, Faculty of Science, University of Malaya, 50603 Kuala Lumpur, Malaysia.

[3]Department of Electronic Engineering, National Changhua University of Education, 500, Taiwan, ROC.

*paulinevcu@hotmail.com

Keywords: Wurtzite InGaN; MREI model; Optical Phonon; Infrared Reflectance

Abstract. Polarized infrared (IR) reflectance measurement was carried out to investigate the optical phonon modes of wurtzite structure $In_{0.92}Ga_{0.08}N$ thin film grown by molecular beam epitaxy. Composition dependence of IR reststrahlen features was observed. Theoretical polarized IR reflectance spectrum was simulated using the standard multilayer optics technique with a multi-oscillator dielectric function model. By obtaining the best fit of experimental and theoretical spectrum, the Brillouin zone center E_1 optical phonon modes together with the dielectric constant, layer thickness, free carriers concentration and mobility were extracted non-destructively. The extracted E_1 optical phonon modes were compared with those generated from modified random element iso-displacement (MREI) model.

Introduction

Wurtzite indium gallium nitride ($In_xGa_{1-x}N$) alloy is an attractive material for practical applications in optoelectronics field. The energy band gap of $In_xGa_{1-x}N$ covers from 0.64 eV [1] (near-infrared) for InN to 3.4 eV [2] (near UV) for GaN. The band gap engineering makes this material highly beneficial in fabrication of photovoltaic cells [3] and blue/green light emitting diodes [4]. In-rich $In_xGa_{1-x}N$ alloy can also be used as thermoelectric material for power generation and solid-state cooling [5].

Detailed knowledge of fundamental material properties such as phonon frequency and dielectric function is important for device design. To understand the device characteristics, many investigations of lattice dynamic in $In_xGa_{1-x}N$ semiconductors have been done [6-15]. Most of the work has been devoted to A_1(LO) and E_2 modes which are usually probed by Raman spectroscopy [6-10]. However, hitherto studies on E_1(TO) and E_1(LO) modes were limited to only Ga-rich InGaN samples [11-13].

In principle, the peculiar feature of an optical phonon mode will appear distinctly in reststrahlen region of infrared (IR) reflectance spectrum only if three conditions are fulfilled [12]. First, the damping for the particular vibration mode is sufficiently small. Second, there is no contribution of strong spectral features of other heterostructure constituent near the mode. Third, the thickness of the material is not too thin. In particular, another possible obstacle in determining the E_1(LO) precisely is the coupling effect between free carrier and longitudinal optical phonon (LOPC).

In this paper, special emphasis is placed on the E_1 optical phonon modes of wurtzite In-rich $In_{0.92}Ga_{0.08}N$ thin film. We adopt both experimental and theoretical approaches to investigate this topic. Modified random element iso-displacement (MREI) model is used as an auxiliary method to predict the harmonic optical phonon modes of wurtzite $In_{0.92}Ga_{0.08}N$. Fourier transform infrared (FTIR) reflectance spectroscopy is used to explore the optical response of the material in the wavenumber range of 400 – 7000 cm^{-1}. Subsequently, the comparison between the experimental result and theoretical prediction of optical phonon mode is made. Finally, the excitations modes resulted from LOPC, i.e., longitudinal optical phonon-plasmon ($LPP_{\pm}$) modes, the carrier density (n) and mobility (μ) are reported.

Experimental Procedure and Theoretical Models

The $In_{0.92}Ga_{0.08}N$ was grown on unintentionally doped (UID) n-type GaN template/*c*-plane sapphire template by Oxford Clusterlab 600 molecular beam epitaxy (MBE). The plasma was operated at typical nitrogen flow of 1 sccm under a discharge power of 240 W. The In and Ga cell temperatures were set at 886 °C and 910 °C, respectively. The $In_{0.92}Ga_{0.08}N$ was grown for 60 minutes at substrate temperature of 525 °C with the growth rate of 0.35 μm/hr. The surface roughness of the thin film as determined by atomic force microscopy (NT-MDT Solver P47) was 10.4 nm. Siemens D5000 high resolution X-ray diffraction spectroscopy was used to investigate the indium composition of thin film through Vegard's relation.

Room temperature *s*-polarized IR reflectance measurement for the range of mid-IR (400-7000 cm^{-1}) was conducted using a FTIR spectrometer (Spectrum GX FT-IR Perkin-Elmer). The *s*-polarization of the incident light beam was selected with the aid of the thallium iodide bromide polarizer. The incident angle of IR light beam was 16° from the surface normal of the sample. An aluminium coating mirror was used as a reference standard. The spectrum was recorded using 32 scans at a resolution of 4 cm^{-1}.

Assume that the optical *c*-axis is parallel to crystal surface normal ($c_{axis} \parallel z$) and perpendicular to direction of propagation ($c_{axis} \perp x$), the component of electric field, *E* in *s*-polarized light rays travels perpendicularly to the *c*-axis. Taking the anisotropy into account, the dielectric function which considers the contributions of lattice vibration (phonon) and free carriers (plasmon) can be expressed as [16, 17]:

$$\varepsilon_{\perp}(\omega) = \varepsilon_{\infty\perp} \prod_{j}^{N} \left(\frac{\omega_{LOj}^2 - \omega^2 - i\omega\gamma_{LOj}}{\omega_{TOj}^2 - \omega^2 - i\omega\gamma_{TOj}} \right)_{\perp} - \left(\frac{\varepsilon_{\infty}\omega_{pj}^2}{\omega^2 + i\omega\gamma_{pj}} \right)_{\perp}, \quad (1)$$

where ω, ε∞, ωTO, ωLO, ωp are the angular frequency, high frequency dielectric constant, transverse optical (TO) phonon mode, longitudinal optical (LO) phonon modes and plasmon mode, respectively. The subscript j represents the specific number of oscillator while γ is the damping coefficient for each mode. By adopting the standard transfer matrix formulation, the *s*-polarized IR spectrum of a five layers system, i.e., vacuum/$In_{0.92}Ga_{0.08}N$/n-$In_{0.92}Ga_{0.08}N$/ *c*-UID GaN/sapphire (Al_2O_3) was simulated. Here, n-InGaN represents the interface electron accumulation layer of InGaN with high density of free carriers. The least-squares curve fitting technique was used to extract the important parameters such as film thickness (d), ε∞, ωTO, ωLO and ωp. To visualize the phonon resonances clearly, first derivative (FD) of the spectrum was performed as well. The ωp and γp can be expressed in terms of free carrier concentration, n and the mobility, μ respectively, i.e., ωp2 = ne2/εoε∞ m* and γp = e/m*μ. The symbol of εo, m* and e are the permittivity in free space, effective mass and electron charge respectively. Assuming that linear composition dependence of effective mass for InGaN, i.e., mInGaN* = xmInN* + (1-x)mGaN*, effective mass, m* of In0.92Ga0.08N is 0.0636 where the value of mGaN*and mInN* are taken from Ref. 24 and Ref. 25, respectively. Prior to fitting procedure, the harmonic optical phonon mode of In0.92Ga0.08N can be predicted by MREI [18]. The required input parameters are ε∞,GaN(InN)=5.2(8.4), ωTO,GaN(InN) = 559(476) cm-1, ωLO,GaN(InN) = 741(593) cm-1, lattice constant aGaN(InN) = 3.1890(3.5378) Å and lattice constant cGaN(InN) = 5.1855(5.7033) Å [19-23]. It is worth to mention that wurtzite InxGa1-xN exhibits one-mode behavior for composition dependence of both A1 and E1 optical phonon modes [14, 15].

Results and Discussion

Figure 1 shows the room temperature *s*-polarized IR experimental spectrum (solid line) and theoretical spectrum (dotted line) of vacuum/$In_{0.92}Ga_{0.08}N$/n-$In_{0.92}Ga_{0.08}N$/*c*-UID GaN/*c*-sapphire for the range of 400-7000 cm^{-1} at the incident angle of 16°. The inset figure displays the FESEM cross-sectional image of $In_{0.92}Ga_{0.08}N$ thin film. According to Ishitani et al., InN sample possesses

interface electron accumulation layer [26]. Hence, we strongly believed that the In-rich sample will exhibit similar characteristics as InN. For this reason, a thin interface electron accumulation layer of n-In0.92Ga0.08N was proposed in our multilayer stack model for the spectrum simulation. The d and $\varepsilon\infty$ of each layer which are sensitive to the non-reststrahlen region (approx. 1000 – 7000 cm^{-1}) can be extracted through simulation; the values were tabulated in Table 1. As shown in Table 1, both the thickness of GaN and the total thickness of InGaN film, i.e., $d(In_{0.92}Ga_{0.08}N) + d(n\text{-}In_{0.92}Ga_{0.08}N) = 0.325$ μm are in a good agreement with FESEM image.

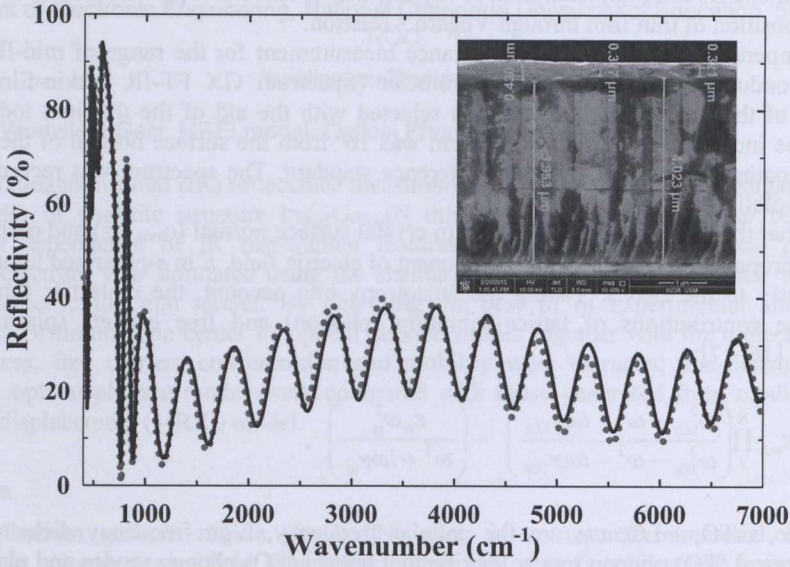

Fig. 1 Room temperature *s*-polarized IR experimental spectrum (solid line) and simulated spectrum (dotted line) of vacuum/$In_{0.92}Ga_{0.08}N$/n-$In_{0.92}Ga_{0.08}N$/*c*-UID GaN/*c*-sapphire for the range of 400-7000 cm^{-1} at the incident angle of 16°. The inset figure displays the FESEM cross-sectional image of $In_{0.92}Ga_{0.08}N$ thin film.

Table 1 The fitting parameters of reflectance spectrum, calculated n and μ for the layer of In0.92Ga0.08N, n-In0.92Ga0.08N and c-UID GaN. The n and μ are in the unit of cm-3 and cm2/Vs respectively.

Layer	d [μm]	$\varepsilon\infty$	ωTO (γTO) [cm-1]	ωLO (γLO) [cm-1]	ωp (γp) [cm-1]	n(μ)
$In_{0.92}Ga_{0.08}N$	0.280	8.0	484.3(10.0) 600.0(15.0)*	594.0(10.0)* 610.0(2.0)	582.0(100.0)	1.93×10^{18} (1467.07)
n-$In_{0.92}Ga_{0.08}N$	0.045	8.0	484.3(15.4)	610.0(2.0)	1995.0(1249.0)	2.26×10^{19} (117.46)
UID GaN	4.040	5.1	558.5 (5.9)	741.5(10.0)	-	-

* Attributed to the defect mode.

Figure 2 displays the room temperature *s*-polarized (a) IR reflectance spectrum and (b) FD reflectance spectrum of vacuum/$In_{0.92}Ga_{0.08}N$/n-$In_{0.92}Ga_{0.08}N$/*c*-UID GaN/*c*-sapphire in the reststrahlen region (approx. 400 – 1200 cm^{-1}). Similarly, the dotted line represents the simulated result and the solid line represents the experimental data. It is evident that the simulated results are in good agreement with experiment for both the reflectance spectrum and the FD reflectance spectrum. In other words, the presence of n-$In_{0.92}Ga_{0.08}N$ is supported by the best-fit results. Based on MREI model, the lattice vibration frequency of wurtzite $In_{0.92}Ga_{0.08}N$ was obtained, namely

ωTO,ideal = 485.63 cm-1 and ωLO,ideal = 606.09 cm-1. Through Clausius-Mossotti relation, the calculated ε∞ of wurtzite In0.92Ga0.08N is 8.1283. Subsequently, these theoretical parameters were used as the initial guess parameters for the IR reflectance spectrum simulation. We found that the fitted optical phonon modes of wurtzite In0.92Ga0.08N (ωTO,exp = 484.3 cm-1 and ωLO,exp = 610 cm-1) agree quite well with the predicted value from the ideal case. Note that for UID GaN layer and sapphire substrate, the initial guess of phonon modes and ε∞ were obtained from Ref. 19 and Ref. 27, respectively. These values are close to those obtained from the present work.

As shown in Table 1, small deviation between the ideal predicted ε∞ and the fitted ε∞ in experiment can be attributed to the surface roughness of the sample (~10.4 nm). Instead of theoretically predicted one-mode behaviour, there is an extra weak mode of In0.92Ga0.08N as indicated by an arrow in Fig 2(a). This feature is likely recognised as the defect mode which presumably arises due to the presence of void component in the layer of In0.92Ga0.08N. For clarity, the optical phonon modes arisen from crystal defects are labeled with an additional symbol * in Table 1. As aforementioned, the sensitivity and accuracy in probing the E1(LO) of In0.92Ga0.08N are low due to the small thickness of the film and LOPC effect, respectively. Hence, the LPP± modes, which are most probably observed in IR reflectance or Raman measurements for samples with significant carrier density, are calculated to provide an alternative reference. If all the damping in the Eq. (1) and the weak defect mode are ignored, a rough estimation of observed LPP modes (i.e., ωLPP, - = 372.74 cm-1, ωLPP, + = 756.23 cm-1 can be determined by using the formula ωLPP, ±2 = 0.5[(ωLO2+ωp2) ± ((ωLO2+ωp2)2 - 4ωp2ωTO2)0.5] [28]. Next, the value of n in the layer of n-$In_{0.92}Ga_{0.08}N$ is greater than the *n* of the bulk layer $In_{0.92}Ga_{0.08}N$ and vice versa for μ.

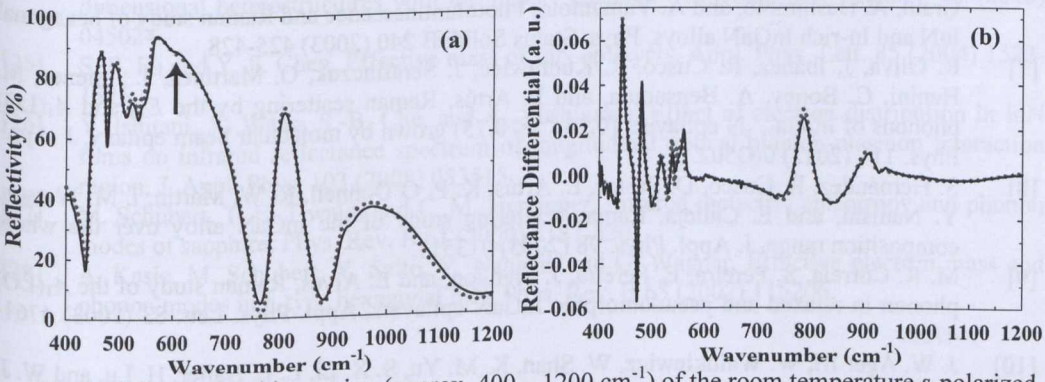

Fig. 2 (a) The reststrahlen region (approx. 400 – 1200 cm^{-1}) of the room temperature *s*-polarized IR reflectance spectrum and (b) its first derivative (FD) reflectance spectrum of vacuum/$In_{0.92}Ga_{0.08}N$/n-$In_{0.92}Ga_{0.08}N$/*c*-UID GaN/*c*-sapphire. The dotted line represents the simulated result and the solid line represents the experimental data. The arrow indicates the extra weak mode due to the defects in the $In_{0.92}Ga_{0.08}N$ thin film.

Conclusion

In summary, we have investigated E_1 lattice vibration properties of wurtzite $In_{0.92}Ga_{0.08}N$ theoretically and experimentally. Based on MREI model, the optical phonon modes of $In_{0.92}Ga_{0.08}N$ were determined, i.e., ωTO,ideal = 485.63 cm-1 and ωLO,ideal = 606.09 cm-1. By fitting the *s*-polarized IR reflectance spectrum, the optical phonon mode of wurtzite $In_{0.92}Ga_{0.08}N$ were determined as ωTO,exp = 484.3 cm-1 and ωLO,exp = 610.0 cm-1. The experimental result is in good agreement with theoretical prediction. As alternative reference, LPP modes, mobility and carrier density of $In_{0.92}Ga_{0.08}N$ thin film were calculated.

Acknowledgements

The first author would like to acknowledge the Ministry of Higher Education Malaysia for My BrainSc scholarship. This work was supported by TWAS Research Grant Programme (Grant No. 11-120 RG/MSN/AS_C: UNESCO FR: 3240262655), and by the Ministry of Higher Education of Malaysia through the Fundamental Research Grant Scheme (Grant No. 203/PFIZIK/6711282).

References

[1] J. Wu, When group-III nitrides go infrared: New properties and perspectives, J. Appl. Phys. 106 (2009) 011101.

[2] J. D. Beach, H. Al-Thani, S. McCray, R. T. Collins, and J. A. Turner, Band gaps and lattice parameters of 0.9 μm thick $In_xGa_{1-x}N$ films for $0 \leq x \leq 0.140$, J. Appl. Phys. 91 (2002) 5190-5194.

[3] S. Valdueza-Felip, A. Mukhtarova, Q. Pan, G. Altamura, L. Grenet, C. Durand, C. Bougerol, D. Peyrade, F. González-Posada, J. Eymery, and E. Monroy, Photovoltaic Response of InGaN/GaN Multiple-Quantum Well Solar Cells, Jpn. J. Appl. Phys. 52 (2013) 08JH05.

[4] A. Khan, K. Balakrishnan, and T. Katona, Ultraviolet light-emitting diodes based on group three nitrides, Nat. Photonics 2 (2008) 77-84.

[5] B. N. Pantha, R. Dahal, J. Li, J. Y. Lin, H. X. Jiang, and G. Pomrenke, Thermoelectric properties of $In_xGa_{1-x}N$ alloys, Appl. Phys. Lett. 92 (2008) 042112.

[6] V. Y. Davydov, A. A. Klochikhin, V. V. Emtsev, A. N. Smirnov, I. N. Goncharuk, A. V. Sakharov, D. A. Kurdyukov, M. V. Baidakova, V. A. Vekshin, S. V. Ivanov, J. Aderhold, J. Graul, A. Hashimoto, and A. Yamamoto, Photoluminescence and Raman study of hexagonal InN and In-rich InGaN alloys, Phys. Status Solidi B 240 (2003) 425-428.

[7] R. Oliva, J. Ibáñez, R. Cuscó, R. Kudrawiec, J. Serafinczuk, O. Martínez, J. Jiménez, M. Henini, C. Boney, A. Bensaoula, and L. Artús, Raman scattering by the E_{2h} and A_1(LO) phonons of $In_xGa_{1-x}N$ epilayers ($0.25 < x < 0.75$) grown by molecular beam epitaxy, J. Appl. Phys. 111 (2012) 063502.

[8] S. Hernández, R. Cuscó, D. Pastor, L. Artús, K. P. O'Donnell, R. W. Martin, I. M. Watson, Y. Nanishi, and E. Calleja, Raman-scattering study of the InGaN alloy over the whole composition range, J. Appl. Phys. 98 (2005) 013511.

[9] M. R. Correia, S. Pereira, E. Pereira, J. Frandon, and E. Alves, Raman study of the A_1(LO) phonon in relaxed and pseudomorphic InGaN epilayers, Appl. Phys. Lett. 83 (2003) 4761-4763.

[10] J. W. Ager III, W. Walukiewicz, W. Shan, K. M. Yu, S. X. Li, E. E. Haller, H. Lu, and W. J. Schaff, Multiphonon resonance Raman scattering in $In_xGa_{1-x}N$, Phys. Rev. B 72 (2005) 155204.

[11] A. G. Kontos, Y. S. Raptis, N. T. Pelekanos, A. Georgakilas, E. Bellet-Amalric, and D. Jalabert, Micro-Raman characterization of $In_xGa_{1-x}N/GaN/Al_2O_3$ heterostructures, Phys. Rev. B 72 (2005) 155336.

[12] A. Kasic, M. Schubert, J. Off, B. Kuhn, F. Scholz, S. Einfeldt, T.Böttcher, D. Hommel, D. J. As, U. Köhler, A. Dadgar, A. Krost, Y. Saito, Y. Nanishi, M. R. Correia, S. Pereira, V. Darakchieva, B. Monemar, H. Amano, I. Akasaki, and G. Wagner, Phonons and free-carrier properties of binary, ternary, and quaternary group-III nitride layers measured by infrared spectroscopic ellipsometry, Phys. Status Solidi C 0 (2003) 1750-1769.

[13] T. R. Yang, M. M. Dvoynenko, Y. F. Cheng, and Z. C. Feng, Far-IR investigation of thin InGaN layers, Physica B 324 (2002) 268-278.

[14] H. Grille, C. Schnittler, and F. Bechstedt, Phonons in ternary group-III nitride alloys, Phys. Rev. B 61 (2000) 6091-6105.

[15] S. Yu, K. W. Kim, L. Bergman, M. Dutta, M. A. Stroscio, and J. M. Zavada, Long-wavelength optical phonons in ternary nitride-based crystals, Phys. Rev. B 58 (1998) 15283-15287.

[16] F. Gervais and B. Piriou, Anharmonicity in several-polar-mode crystals: adjusting phonon self-energy of LO and TO modes in Al_2O_3 and TiO_2 to fit infrared reflectivity, J. Phys. C 7 (1974) 2374-2386.

[17] R. Kroon, The classical oscillator model and dielectric constants extracted from infrared reflectivity measurements, Infrared Phys. Technol. 51 (2007) 31-43.

[18] D. L. Peterson, A. Petrou, W. Giriat, A. K. Ramdas, and S. Rodriguez, Raman scattering from the vibrational modes in Zn1-xMnxTe, Phys. Rev. B 33 (1986) 1160-1165.

[19] T. Yang, S. Goto, M. Kawata, K. Uchida, A. Niwa, and J. Gotoh, Optical properties of GaN thin films on sapphire substrates characterized by variable-angle spectroscopic ellipsometry, Jpn. J. Appl. Phys. 37 (1998) L1105-L1108.

[20] B. E. Foutz, S. K. O'Leary, M. S. Shur, and L. F. Eastman, Transient electron transport in wurtzite GaN, InN, and AlN, J. Appl Phys. 85 (1999) 7727-7734.

[21] V. Y. Davydov, Y. E. Kitaev, I. N. Goncharuk, A. N. Smirnov, J. Graul, O. Semchinova, D. Uffmann, M. B. Smirnov, A. P. Mirgorodsky, and R. A. Evarestov, Phonon dispersion and Raman scattering in hexagonal GaN and AlN, Phys. Rev. B 58 (1998) 12899-12907.

[22] V. Y. Davydov, V. V. Emtsev, I. N. Goncharuk, A. N. Smirnov, V. D. Petrikov, V. V. Mamutin, V. A. Vekshin, S. V. Ivanov, M. B. Smirnov, and T. Inushima, Experimental and theoretical studies of phonons in hexagonal InN, Appl. Phys. Lett. 75 (1999) 3297-3299.

[23] M. A. Moram and M. E. Vickers, X-ray diffraction of III-nitrides, Rep. Prog. Phys. 72 (2009) 036502.

[24] S. Gökden, R. Tülek, A. Teke, J. H. Leach, Q. Fan, J. Xie, Ü. Özgür, H. Morkoç, S. B. Lisesivdin, and E. Özbay, Mobility limiting scattering mechanisms in nitride-based two-dimensional heterostructures with the InGaN channel, Semicond. Sci. Technol. 25 (2010) 045024.

[25] S. P. Fu and Y. F. Chen, Effective mass of InN epilayers, Appl. Phys. Lett. 85 (2004) 1523-1525.

[26] Y. Ishitani, X. Wang, S.-B. Che, and A. Yoshikawa, Effect of electron distribution in InN films on infrared reflectance spectrum of longitudinal optical phonon-plasmon interaction region, J. Appl. Phys. 103 (2008) 053515.

[27] M. Schubert, T. E. Tiwald, and C. M. Herzinger, Infrared dielectric anisotropy and phonon modes of sapphire, Phys. Rev. B 61 (2000) 8187-8201.

[28] A. Kasic, M. Schubert, Y. Saito, Y. Nanishi, and G. Wagner, Effective electron mass and phonon modes in n-type hexagonal InN, Phys. Rev. B 65 (2002) 115206.